



Biogenic Synthesis of Zinc Oxide Nanoparticles with Leaves and Cones Concentrate of *Cupressus Arizonica* and Assessment of Photocatalytic and Antibacterial Efficiency

Mahmure USTUN OZGUR^{1*}, Ebru ORTADOGLU¹, Burak ERDEMIR¹, Mine AYDIN KURC²

¹Yildiz Technical University, Faculty of Science and Art, Department of Chemistry, 34220 Istanbul, Türkiye

²Tekirdag Namik Kemal University, Faculty of Medicine, Department of Medical Microbiology, Tekirdag, 59030, Türkiye

Highlights

- First report on biosynthesis of ZnO NPs using leaf and cone concentrate of *Cupressus arizonica*
- This study demonstrates economical, simple and fast synthesis procedure of multifunctional ZnO NPs.
- The nanoparticles could decolorize dyestuffs with efficiency more than 53% (from 53% to 100%).
- ZnO NPs demonstrated antibacterial effectiveness against bacteria.

Article Info

Received: 17 Agu 2023

Accepted: 05 Feb 2024

Keywords

Zinc oxide
Cupressus arizonica
Photocatalyst
Antibacterial
Textile dye

Abstract

Among the metal oxide nanoparticles, zinc oxide (ZnO) has recently been cited as the new material of the future due to its unique properties and wide application areas. In this study, we offer a simple technique for the production of extremely stable ZnO nanoparticles (CA-ZnO NPs) using the aqueous and ethyl alcohol (1/1, v/v) extract of *Cupressus arizonica* (CA, Blue cypress) leaves and cones and zinc acetate (Zn-Ac) salt. The structure of the produced CA-ZnO NPs was elucidated and nanoparticles were used as a photocatalyst for the removal of textile dyestuffs. The particle sizes of CA-ZnO NPs calcined at different temperatures (60°C, 150°C, and 400°C) increased from 20 nm to 50 nm. Produced CA-ZnO NPs were used to investigate photocatalytic degradation of Basic Yellow (BY28), Basic Violet 39 (BV39), Methylene blue (MB), Brilliant Blue (BB3) and Basic Red 46 (BR46) in aqueous solution under UV- light and daylight irradiation. After stirring dye solutions containing CA-ZnO NP for one hour in darkness and 7 hours under UV- light, decolorization rates varied from 53% to 100%. Decolorization of the dyestuff molecules follows the pseudo first-order kinetics. Produced CA-ZnO NPs showed antibacterial efficiency against *Escherichia coli* and *Staphylococcus aureus*. CA-ZnO NPs formed zones ranging from 10 mm to 11 mm against gram+ and gram- bacteria. Green production of ZnO NPs utilizing *Cupressus arizonica* plant extract can replace chemical methods, and the resulting CA-ZnO NPs can be used in industries like water purification. This eco-friendly biogenic synthesis method is a new, inexpensive and useful technique suitable for large scale.

1. INTRODUCTION

Green production technique, which is used in the production of nanoparticles and in which plants are used, is an alternative and eco-friendly method that eliminates the use of substances detrimental to the health of people and the environment. Recently, different parts of many plants have been widely used in the biogenic synthesis of nanoparticles, because they contain metabolites that serve as reducing, coating, and stabilizing agents, such as phenols, flavonoids, alkaloids, alcohols, terpenoids, sugars, and proteins. At the same time, these phytochemicals act as a good coating (enhancing their properties by enveloping nanoparticles) and stabilizing compounds. Therefore, for the production of nanoparticles, researchers focused on all the plant species that contain phytochemicals in their roots, leaves or flowers that will reduce metal ions to metal nanoparticles and stabilize them. In most of the nanosynthesis studies, it is aimed that the nanostructures obtained have a certain size and morphology. Thanks to the chemical and physical technologies used in nanoparticle production for a long time, small particles with high solubility can be produced in a short time, but newer technologies need to be researched due to their weak particle stability, high toxic content, and

*Corresponding author, e-mail: mozgur@yildiz.edu.tr

expensive technologies [1]. In this respect, "green nanotechnology", which includes environmentally friendly, economical, and non-hazardous biological techniques, is at the forefront today [2]. Plants that are easily available and abundantly available are generally used as plants, and it is known that the obtained nanoparticles are more stable [3]. Nanoparticle production methods using different parts of plants are an alternative to traditional chemical and physical production methods. It is well known that biological methods of producing nanoparticles have become important due to their simplicity, eco-friendliness, and extensive antibacterial properties. Some examples of studies conducted in the last 10 years that produced ZnO by green synthesis using various plant sources are given in Table 1.

Table 1. Reaction conditions and some data for ZnO NPs produced using different plants

Stabilizing Agent, Plant Part	Precursor	Research Purpose	Reaction Conditions	Phytochemicals	Particl Size (nm)	Morphology	Ref.
<i>Geranium wallichianum</i> , leaves	Zn (NO ₃) ₂ . 6H ₂ O	anticancer, antileishmanial, antimicrobial, biocompatibility	60°C, 2 h dried 100°C, 3 h	Ursolik Acid, Herniarin, Stigmasterol	18	hexagonal	[4]
<i>Camellia sinensis</i> , leaves	Zn (NO ₃) ₂ . 6H ₂ O	photocatalytic	350±10°C 4 min	Aromatic structures, C-C, C=O, C-H	9-17.5	variable	[5]
<i>Raphanus sativus</i>	Zn (CH ₃ COO) ₂ . 2H ₂ O	antimicrobial activity	2 h, 50°C	Lukoizinolat, Miyrozinaz, Isothiocyanate	60-100	spherical	[6]
¹ <i>Matricaria chamomilla</i> L., flowers ² <i>Oleaeuropaea</i> , leaves ³ <i>Lycopersicon esculentum</i> M., fruits	1M ZnO	antibacterial, photocatalytic activities	60°C	Saponins, Alkaloids, Flavonoids	¹ 48.2 ² 65.4 ³ 61.6	cubic	[7]
<i>Camellia sinensis</i> , leave	Zn (CH ₃ COO) ₂ . 2H ₂ O	antimicrobial, medicine	150°C, 5-6 h	-----	853	aggregate	[8]
<i>Euphorbia hirta</i> , leaves	Zn (NO ₃) ₂ . 6H ₂ O	photocatalytic efficiency	70°C, 20min and then 80°C, 6 h	Alkaloid, Flavanoid, Saponins	20-25	partial spherical	[9]
<i>Calliandra haematocephala</i> , leaves	Zn (NO ₃) ₂ . 6H ₂ O	photocatalytic efficiency	80°C, 2 h and then 90°C, 10 h	Acetylamino, Hydroxy (Mono and di) derivatives	19.45	hexagonal, wurtzit, flower	[10]
<i>Nephelium lappaceum</i> L., shell	Zn (NO ₃) ₂ . 6H ₂ O	textile, antibacterial activities	80°C, 2 h	Polyphenols, O-H, H-O-H	50.95	needle agglomerate	[11]
<i>Agathosma betulina</i> , dry leaves	Zn (NO ₃) ₂ . 6H ₂ O	antioxidant and cytotoxic properties	room temp, 6h, dried at 80 °C	O-H	12-26	semi-spherical, agglomerate	[12]
<i>Celosia Cristata</i> , leaves	Zn (CH ₃ COO) ₂ . 2H ₂ O	photocatalytic degradation, antibacterial effect	at 40 °C 120 min, at 300°C, 2 h	Phenols, Flavonoids, Carbohydrates Alkaloids, Tannins	22-27	variable	[13]
<i>Cupressus arizonica</i> , cones and leaves	Zn (CH ₃ COO) ₂ . 2H ₂ O	photocatalytic degradation, antibacterial effect	at 60 °C 120 min, at 400°C, 2h	Tannin, Gallic acid, Caffeic acid	20-50	variable	This study

Footnotes: 1, 2 and 3 refer to the different plants were used.

Biogenically produced nano-sized crystal metal oxides have become one of the most striking subjects of the scientific world, because they are produced as small particles with a large surface area that are appropriate for biological applications [14]. Inorganic antibacterial substances are important as they have potential application areas in sectors such as food, packaging, cosmetics, pharmaceuticals and health. Zinc oxide, which is accepted as GRAS (generally considered safe) metal oxide by US Food and Drug Administration (FDA) [15] is among the promising materials that attract notice because of its outstanding and interesting features, especially because it is suitable for the production of nano-sized particles [16]. ZnO nanoparticles produced by biosynthesis can be applied to a number of different fields, including antimicrobial applications, wastewater facilities, degradation of toxic compounds and insecticides [17]. The antibacterial characteristics of biosynthesized ZnO NPs are by far their most noticeable feature. These particles are the perfect antibacterial agent for preventing bacterial infections because of their smaller size and larger surface area. Research on this subject is not sufficient and still continues. ZnO has a biocidal effect and potent antibacterial capacity due to its physiochemical properties and biocompatibility [18]. Thanks to their small size, ZnO nanoparticles can easily interact with biological molecules. Another reason why ZnO nanoparticles are frequently preferred is that ZnO has a much more stable and longer-lasting structure compared to organic-based disinfectants and antibacterial agents. It has also been found that bioproduced nanoparticles show better antibacterial efficiency compared to chemically produced nanoparticles [9]. In the results of the researchers, it has been seen that ZnO nanoparticles can enter bacterial surfaces and / or bacterial core. Nowadays ZnO is recognized as an antibacterial substance and shows significant antibacterial activities on a wide variety of bacterial species [19]. Use of the ZnO nanoparticles in the paint production gives to the paint anti-odour, UV absorbing and antibacterial properties. When ZnO nanoparticles are incorporated into materials such as plastics, they become useful antibacterial and antifungal agents. Again, when used in the production of packages that protect and increase the shelf life of foods, they ensure that the products gain antibacterial properties for a long time and ensure that the surfaces and products are clean and hygienic. ZnO NPs, which have an important place in agriculture, can also be used successfully as fertilizers and pesticides [20]. Within the framework of these results, the bioproduce of antibacterial ZnO NPs is important and one of our aims in this research is the produce of ZnO nanoparticles with this feature. Industrial wastewater containing dyestuffs is one of the leading causes of pollution of water resources. These dyestuffs, which are toxic as well as threatening human health and the ecosystem, are resistant to heat and sunlight for a long time. Many classical chemical and physical methods are used in the industry for the treatment of dyestuffs before they are discharged to the environment, and these procedures have been developed along with developing technology. In the last years, zinc oxide as a photocatalyst has attracted great attention among semiconductors due to its new technology in reducing environmental pollution [21, 22].

Cupressus arizonica (Blue cypress) is an evergreen blue tree that can grow up to 0-15 m. The essential oil obtained from its branches and leaves contains tannin and cypress camphor and is very useful and used externally. Cypress leaf shoots and cones are used to make tea, tincture, essential oil and natural medicine [23]. Contamination of water with colored substances such as dyestuff is of environmental concern due to their toxicity and causes carcinogenic effects on aquatic life and humans. These dyestuffs are released into water bodies from wastewater of various industries such as food, cosmetics, paint, textile, paper, and others, which cause water pollution.

In this study, our aim is to produce and characterize of ZnO NPs by green technology using alcoholic and aqueous concentrate of the leaves and cones of *Cupressus arizonica* plant and zinc acetate salt, and also to investigate their antibacterial and photocatalytic activities. In this study, the photocatalytic degradation of BY28, BV39, MB, BB3 and BR46 textile dyestuffs under different conditions (pH, daylight and UV- light irradiation time, initial dyestuff concentration, amount of photocatalyst) was investigated by using the produced CA-ZnO NPs.

2. MATERIAL and METHOD

2.1. Instruments and Materials

$\text{Zn}[\text{CH}_3(\text{COO})]_2 \cdot 2\text{H}_2\text{O}$ (zinc acetate dihydrate) was purchased from Sigma-Aldrich. 500 mL of distilled water were used to dissolve 5 g of zinc acetate dihydrate (Zn-Ac), which was then incubated for 15 minutes at 30°C in an ultrasonic bath. Both ethyl alcohol and sodium hydroxide (Sigma, St. Louis, MO, USA) were of analytical quality. Using distilled water, stock dyestuff solutions were made at a concentration of 100 µg/mL. Leaves and cones of the *Cupressus arizonica* plant were collected from the garden of Yıldız Technical University in Istanbul (Figure 1).



Figure 1. Images of the plant *Cupressus arizonica* (Blue cypress)

All spectral measurements and data processing were performed using a double beam Shimadzu UV-1800 spectrophotometer (Japan). Derivative spectra of the absorption spectra recorded between 300 nm and 750 nm were obtained using UV- probe 2.35 software. High-resolution transmission electron microscopy examinations were performed using the JEOL JEM 2100 HRTEM. An Orius SC200D CCD camera, Model 833 Gatan, was utilized for taking pictures. The particles were sonicated with ethanol, and then they were put on copper TEM grids coated with carbon support film (Electron Microscopy Sciences, CF200-Cu, 200 mesh). The SEM studies were carried out using the JEOL JSM 6510-LV SEM and the JEOL JSM 6335F FEG-SEM. After a few drops of particulate ethyl alcohol mixture were dropped on the carbon tape, investigations were made at 15 kV acceleration voltage. For functional group analysis, a Perkin Elmer FT-IR spectrophotometer was used to record the FT-IR spectra of aqueous and ethyl alcohol extracts of the CA leaves, cones, leaves and cones mixture and CA-ZnO NPs. To perform photocatalytic degradation studies, a specially designed setup comprising four Philips (total 32 W) TL 8W Actinic BL UVA lamps with a length of 32.5 cm was utilized.

2.2. Preparation of Extract of *Cupressus arizonica* Leaves and Cones

Deionized water was used to wash the *Cupressus arizonica* plant's leaves and cones. The cleaned samples were chopped into small pieces using a blender. For the biogenic compound extraction, 50 g of finely chopped CA leaves and cones were weighed, added to a 500 mL beaker containing 300 mL of ethyl alcohol and distilled water (1:1, v:v, mL/mL), and stirred for 60 minutes at 80°C at 250 rpm using a magnetic stirrer. To get rid of any suspended particles, following 10 minutes centrifugation at 4000 rpm, the extract was filtered through Whatman filter paper (No. 2). Filtrate was kept at +4°C in the dark for a month's worth of future experiments. Same procedure was applied to the leaves and cones separately using water and ethyl alcohol for extraction.

2.3. Production of ZnO NPs

To produce CA-ZnO NPs, a 250 mL flask filled with 50 mL of the aqueous: ethanolic (1:1, v/v) extract of the CA leaf and cones mixture was heated to 60°C. Using a magnetic stirrer, 50 mL Zn-Ac solution was added dropwise and stirred for an hour at 60°C. The pH of the reaction medium was adjusted to 12 with 2 M NaOH solution and then stirred for another 3 hours. During the reaction period, the solution's color was seen to change from light brown to greenish- white, signifying the formation of CA-ZnO NPs. Figure 2 demonstrates the stages of biosynthesis. The colloidal solution was refrigerated at +4°C for 12 hours in order to obtain a clear solution and to finish the reaction. The greenish- white suspension was centrifuged at 4000 rpm for 20 min. Produced CA-ZnO NPs were washed twice with distilled water and twice with

ethyl alcohol to remove impurities and centrifuged at 4000 rpm for ten minutes in each case to separate the nanoparticles. The precipitate was dried in an oven at 60°C before being calcined in a muffle furnace for two hours at 400°C to convert the generated Zn(OH)₂ and its residues to ZnO. The prepared powder CA-ZnO NPs was stored at room temperature in a desiccator for use in subsequent experiments. For the spectrophotometric measurements, 0.001 g of CA-ZnO NPs was weighed, diluted with water to a volume of 10 mL, and stirred in an ultrasonic bath set at 40°C for 30 minutes. The absorption spectrum of the solution was recorded in the range of 200 nm - 450 nm. The same study was repeated using ethyl alcohol as solvent.

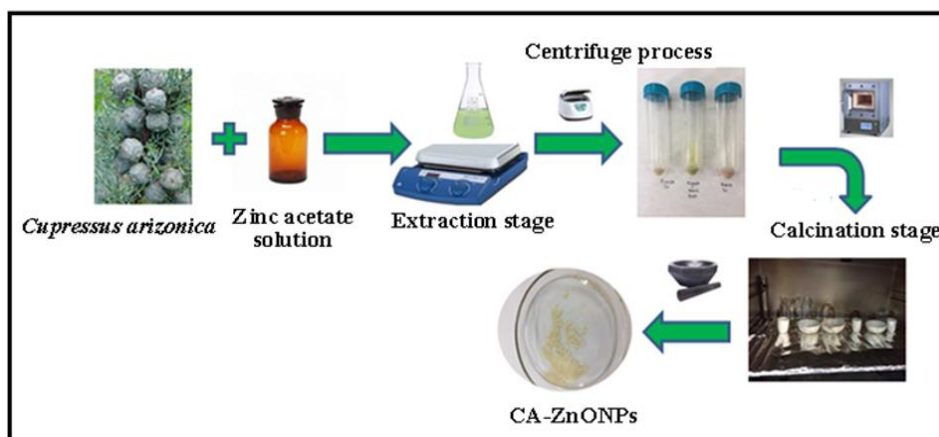


Figure 2. Biosynthesis Stages

2.4. Characterization of CA-ZnO NPs

FT-IR spectrum peaks obtained in the range of 4000cm⁻¹- 400 cm⁻¹ and the UV-Vis absorption peaks obtained in the wavelength range of 200 nm - 450 nm were used to verify the biosynthesis of CA-ZnO NPs. The synthesized CA-ZnO NPs' surface morphology was ascertained using TEM, HR-TEM, and SEM analyses.

2.5. Use of Produced CA-ZnO NPs as Photocatalyst

In order to solve to the global pollution caused by organic pollutants, which are now a serious threat to both human health and the environment, photocatalysis is a promising technology. Studies on this technology have increased recently as an effective wastewater treatment method because it provides the complete chemical conversion of organic pollutants into non-toxic or less toxic products. Within the present study, photocatalytic degradation of BY28, BV39, MB, BB3 and BR46 dyestuffs which are utilized within the textile industry and environmentally toxic in aqueous solution was examined.

In the photocatalytic reactions, ZnO nanoparticles (CA-ZnO NPs, 50 nm in size), synthesized with the solution obtained by the extraction of leaves and cones together in aqueous-alcoholic medium and calcined for two hours at 400°C, were used. The photo-decolorization efficiency was examined under both daylight and UV- light.

Formulas and colors of the dyestuffs used in this study are given in Figure 3. A fixed amount of catalyst consisting of a dyestuff solution of 10 µg/mL and 0.05 g of CA-ZnO NPs was used in the experiments. Each reaction solution's total volume was maintained at 30 mL. For one hour, the reaction mixture was agitated in the dark in order to achieve the liquid/solid phase balance. Thereafter, it was stirred for 7 h while being exposed to UV- light. While the dyestuff solutions were mixed under UV- light, samples were taken from the environment every hour and absorption and first derivative absorption spectra were recorded in the wavelength range of 300 nm - 750 nm. Using the relevant calibration curves and the measured derivative absorbance values, the degree of decolorization of the solutions was computed. The trials were also repeated

under the same conditions in daylight. In addition, the experiments were repeated under the same conditions under daylight and UV- light without using ZnO photocatalyst only with 10 µg/mL dyestuff solution.

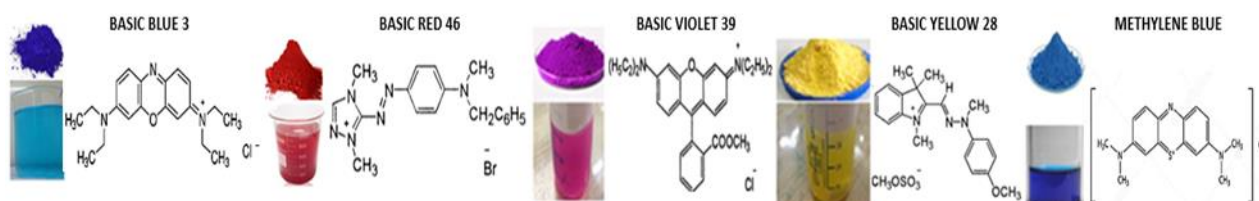


Figure 3. Visuals of dyestuff formulas and colors

2.6. Studies on Antibacterial Activity

For the microbial assay, the modified Kirby-Bauer disk diffusion method was used [24]. Standard strains of gram-positive *Staphylococcus aureus* (ATCC 29213) and gram-negative *Escherichia coli* (ATCC 25922) bacteria were used to assess the antibacterial potency. The bacteria's stock cultures were added to Nutrient Agar (NA) and then activated by being incubated at 37°C for 18-24 hours. Following the period of incubation, Mueller Hinton Broth (MHB) medium was used to standardize the bacterial inoculum to 0.5 McFarland units, or roughly 108 CFU/mL. Sterile cotton swabs were then used to apply bacterial suspensions to Mueller Hinton Agar (MHA) plates. After that, each Petri-plate had a well (6 mm) drilled into it using a sterilized cork borer. The wells that were drilled in solid media received additions of 100 µL concentrations of CA-ZnO NPs solutions. The plates were then kept for a further 18 to 24 hours at 37°C. At the end of the incubation period, the diameter of the inhibition zone was measured in millimeters.

3. THE RESEARCH FINDINGS and DISCUSSION

3.1. Mechanism for the Green Production of CA-ZnO NPs

Figure 4 depicts the likely reaction mechanism for the generation of the CA-ZnO NPs. The production of CA-ZnO NPs involves two steps: the first involves producing Zn (OH)₂ from Zn-AC solution and CA extract, and the second involves calcination of this product to yield CA-ZnO NPs. In the accepted mechanism, the CA extract contains the biogenic molecules (rich in functional groups such as hydroxyl and carboxyl) such as tannin, gallic acid and caffeic acid found in *Cupressus arizonica*. These phenolic groups contribute to the transformation of Zn-AC to Zn (OH)₂. A greenish-white precipitate was formed when tannin, gallic acid, caffeic acid and other biogenic molecules in the structure of the CA plant were exposed to metal ions. This suggests that the reaction has already taken place [25, 26]. By drying the final product and calcination it in a muffle furnace at 400°C, white CA-ZnO NP nanoparticles were formed.

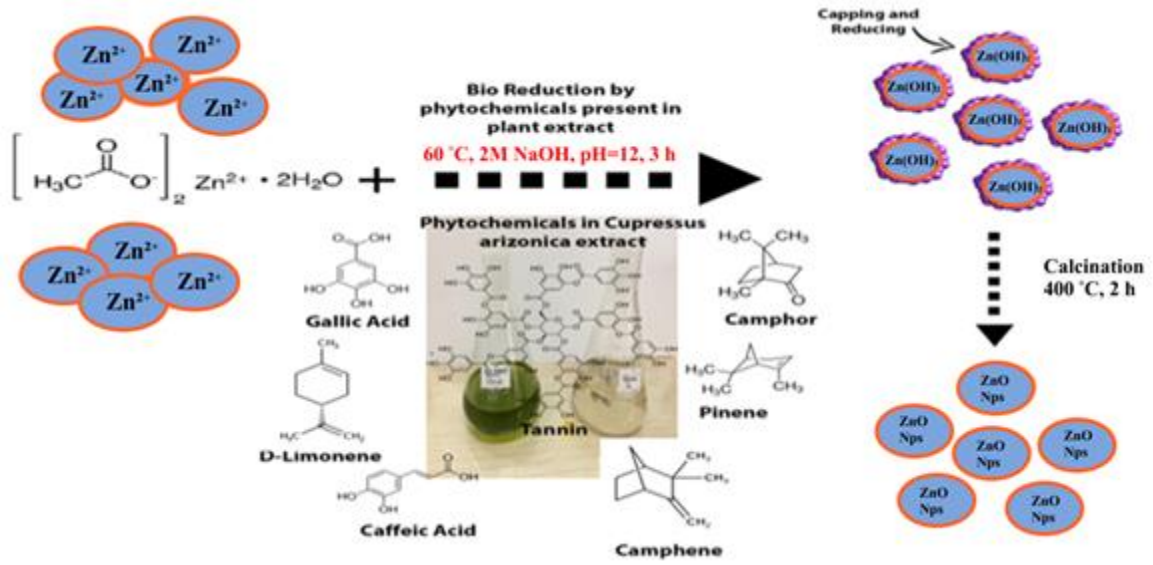


Figure 4. Proposed mechanism for the reaction in green CA-ZnO NP production

3.2. Characterization of CA-ZnO NPs

An approach used to assess the optical characteristics of nanoparticles is UV-Vis spectroscopy. Due to quantum restrictions, semiconductor nanoparticles have different optical properties from their bulk counterparts. The CA- ZnO NPs' absorption spectra were taken between the wavelengths of 200 nm and 450 nm. In this search, UV-Vis and FT-IR data support the production of CA-ZnO NPs from aqueous ethanolic extract of leaves and cones of CA plant by environmentally friendly method. Greenish white color was first indication of the production of CA-ZnO NPs meanwhile it was approved by surface plasmon resonance (SPR) band obtained in the wavelength range of 340 nm-380 nm. The SPR band of the produced CA-ZnO NPs showing a distinct peak at 365 nm confirms the formation of ZnO nanoparticles (Figure 5). It is apparent that the value found is in line with the previously reported literature findings [27, 28].

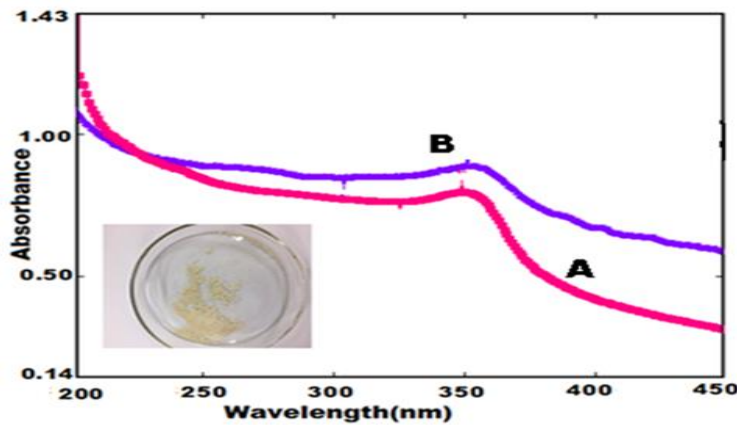


Figure 5. Absorption spectra of CA-ZnO NPs (calcined at 400°C), A: ethanolic, B: aqueous media, inset; visual of produced CA-ZnO NPs

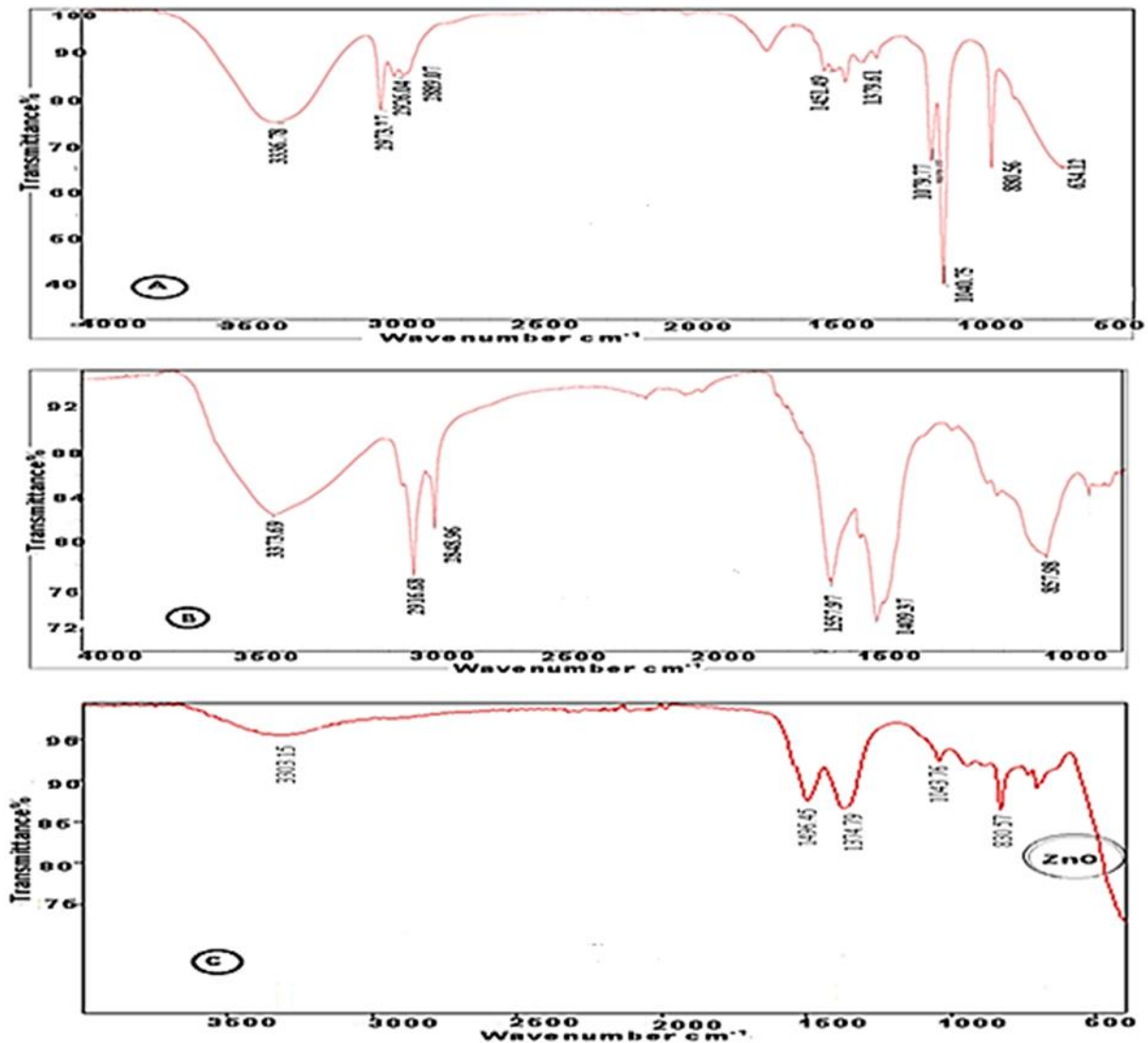


Figure 6. FT-IR spectra of (A) aqueous-alcoholic extract of the cones and leaves mixture of CA plant, CA-LCEWE (B) CA-ZnO NPs dried at 60°C for 2 h and (C) CA-ZnO NPs calcined at 400°C for 2 h

FT-IR technique was used to research for possible functional groups of aqueous-alcoholic extract of leaves and cones of CA plant (CA-LCEWE, Figure 6A) and biosynthesized CA-ZnO NPs (Figure 6B and 6C). We can attribute the peaks seen in Figure 6A as follows: 3336.78 cm^{-1} (-OH stretching), 2973.27 cm^{-1} , 2926.04 cm^{-1} and 2889.07 cm^{-1} (alkane C-H stretching), 1451.49 cm^{-1} and 1379.61 cm^{-1} (alkane C-H bending), 1324.16 cm^{-1} (O-H bending), 1272.82 cm^{-1} , 1079.77 cm^{-1} and 1040.75 cm^{-1} (C-O stretching), 880.56 cm^{-1} (C-H bending). The hydroxyl group of phenol exhibits a broad peak of stretching vibration between 3000 cm^{-1} and 3600 cm^{-1} . The peak at 3336 cm^{-1} is assigned to the O-H stretching mode of physisorbed molecular water and can be attributed to the characteristic functional group alcohol O-H stretching vibration (likely originating from the residual alcohol) [29]. Comparing these peaks with the spectra of CA-ZnO NPs, it is seen that there is a decrease in the peak broadening of CA-ZnO NPs. This band is significantly reduced in Figure 6C and shows a considerable dissociation of the hydroxyl group after calcination. Peaks in the CA-LCWE spectrum between 3100 cm^{-1} and 2800 cm^{-1} are assumed to be tensile vibrations of C-H molecules (CH_3 , CH_2 , etc.). The bands at 1040 cm^{-1} and 634 cm^{-1} , respectively, show the presence of the C-O stretching vibration of alcohol and the C-H vibration of the -CH=CH of the ethylene system. The following factors are responsible for the peaks in Figure 6B: Alkane C-H stretching = 2916.68 cm^{-1} , 2848.96 cm^{-1} , -OH stretching = 3373.69 cm^{-1} , and C=C stretching = 1557.97 cm^{-1} . According to Figure 6B, the two low-intensity peaks at approximately 2916 cm^{-1} and 2848 cm^{-1} matched the symmetric and asymmetric C-H of the aliphatic group. The bands seen in the 1000 cm^{-1} –1600 cm^{-1} range are assumed to be caused by the C=O and C=C stress vibrations of the aromatic groups found in CA-

LCWEE and CA-ZnO NPs (Figure 6A–C). Metal oxides usually vibrate at frequencies lower than 1000 cm^{-1} . Smaller peaks at 900 cm^{-1} – 700 cm^{-1} were also assigned to the aromatic bending vibration of C–H group. The bonds at 1557 cm^{-1} and 1496 cm^{-1} C=C stretch in aromatic rings and C=O stretch in polyphenols are shown in Figures 6B and 6C. The C–OH bond is responsible for 1409 cm^{-1} vibration, the alkane group for 1374 cm^{-1} C–H bending, and the C–H bending for 839.03 cm^{-1} vibration. The peaks shown in Figure 6C can also be attributed to the following: -OH stretching at 3303.15 cm^{-1} , alkane C–H bending at 1496.45 cm^{-1} and 1374.79 cm^{-1} , and a second peak at approximately 480 cm^{-1} (Zn–O stretching vibration). It has been reported in the literature that the absorption peaks seen at lower energy region in the range of 400 cm^{-1} – 600 cm^{-1} belongs to the characteristic stretching vibration of Zn–O bond [30]. Prominent peak at around 470 cm^{-1} indicates the formation of CA-ZnO NPs. These findings concur with the UV-Vis absorption finding. Significant variations in peak intensity, shape, and location following the synthesis of CA-ZnO NPs show that the functional groups of the CA plant contributed to the formation and coating of nanoparticles. The values obtained in this study are similar to those which the other studies have shown, when evaluated on the basis of literature findings [31–33].

As seen in Figure 7 and 8, it is impossible to count the particles as they do not have sharp edges and do not have a typical morphology. TEM images taken at 100 nm scale of ZnO NPs biosynthesized at optimum conditions and calcinated different temperatures were given in Figure 8 and HR-TEM images (with different magnification) of CA-ZnO NPs, calcinated at 400°C , were given in Figure 9. As you can see, as temperatures rise from 60°C to 150°C and 400°C the particle size also gets bigger with smaller particles reaching a diameter of 50 nm .

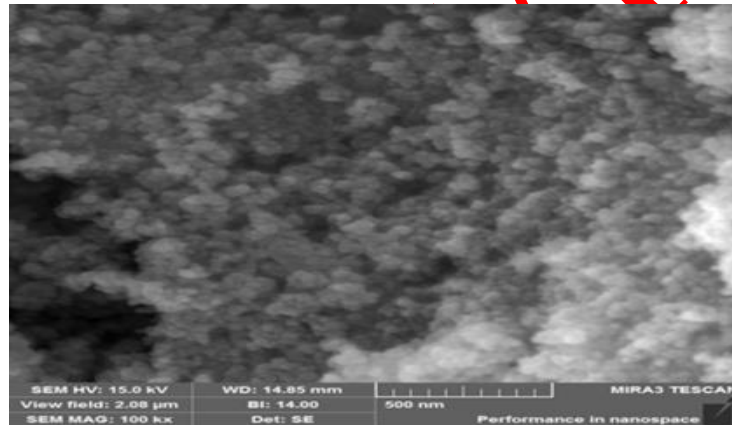


Figure 7. SEM Images taken at 500 nm scale of biosynthesized CA-ZnO NPs

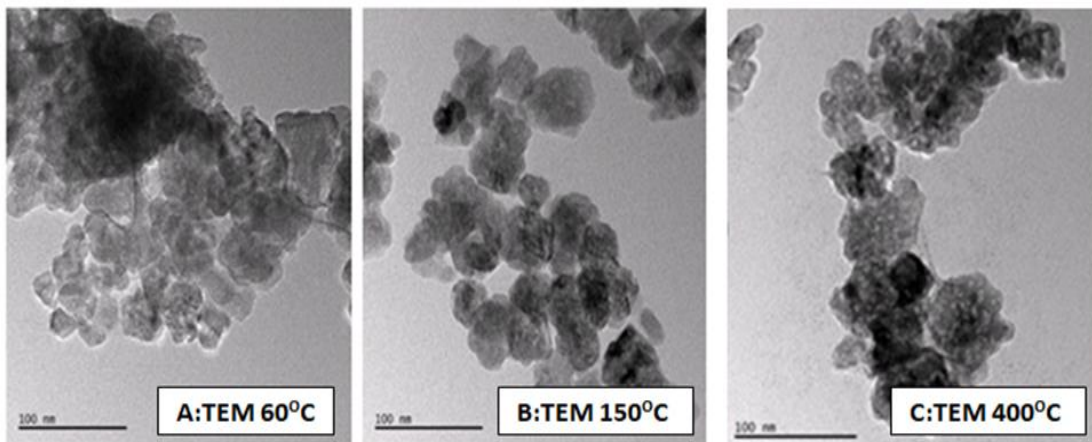


Figure 8. TEM images taken at 100 nm scale of CA-ZnO NPs biosynthesized at optimum conditions and calcinated different temperatures

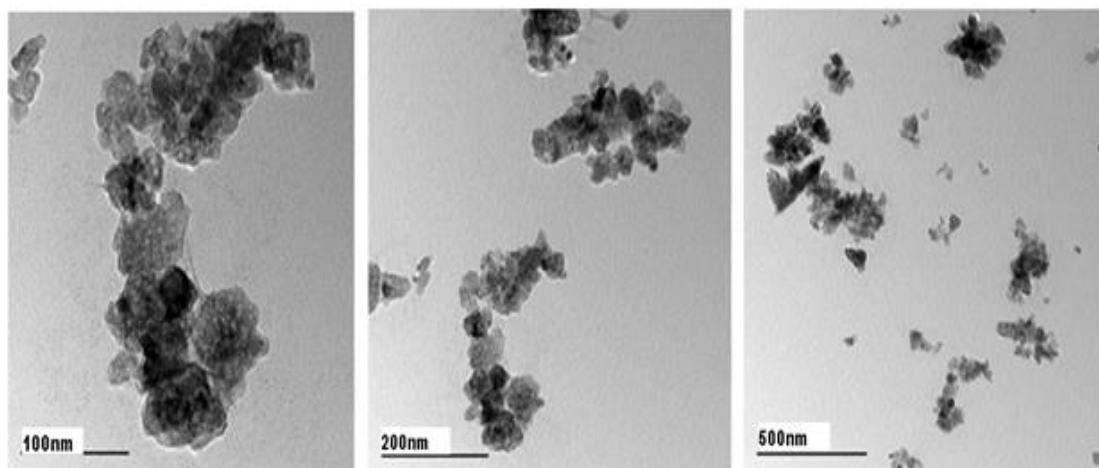


Figure 9. HR-TEM images (with different magnifications) of CA-ZnO NPs calcined at 400°C

3.3. Photocatalytic Efficiency of CA-ZnO NPs

In recent years, photocatalysis has been a fascinating subject for the degradation of organic pollutants. Photocatalysis, which converts photonic energy into chemical energy, is a green method for converting organic pollutants into mineral products because of its ease of use and low energy requirements. The design and synthesis of new semiconductor materials had been the subject of extensive research in recent years with the goal of creating photoreactors that will improve photocatalysis efficiency. Usually, the efficiency of the photocatalysis operation mainly depends on the reactors, bandgap of the photocatalyst and to semiconductor materials. The most widely used photocatalysts are TiO₂, ZnO, Fe₂O₃ and CdS, etc. In photocatalysis on semiconductors, an excited electron (e⁻) and a positive hole (h⁺) are formed by the absorption of light of a larger energy from the band gaps, followed by reduction and oxidation by e⁻ and h⁺, respectively. In typical photocatalytic reactions, electron hole pairs (e⁻/h⁺) are created when catalytic semiconductor particles (catalysts or substrates) were illuminated with photons or light energy (ultraviolet lamps, xenon lamps, or even visible light) [34, 35]. By absorbing light energy, an excited electron/hole pair is generated. Due to their activated case, the electron/hole pair actualizes chemical oxidation and reduction as if they were highly reactive reagents in a chemical reaction (Figure 10). For the photocatalyst to actuate as quickly and sustainably as possible, both the oxidation and reduction reactions have to take place simultaneously. Recently, photocatalysis has been studied as an alternative or complementary process to existing drinking water treatment techniques, and there is an increasing interest in the studies.

In this work, measurements of the decolorization of dye solutions under UV- light and daylight were made to assess the photocatalytic activity of CA-ZnO NPs. The fundamentals of the photocatalysis procedure, which is carried out by a series of reactions on the surface of CA-ZnO NPs, are shown in Figure 10. The possible mechanism is schematically given in Figure 10 and the chemical reaction steps for the photocatalytic operation are given below. The photocatalytic efficiency of semiconductors is explained by the band theorem. The mechanism of a typical photocatalytic process consists of four steps: surface oxidation-reduction reactions, charge separation, translocation, and photoexcitation. At this point, organic pollutants that are physically bonded to the zinc oxide surface, where photocatalytic degradation takes place, are attacked by free radicals produced by photoexcitation, particularly the hydroxyl radical. They quickly convert pollutants into harmless substances such as CO₂ and H₂O [36, 37].

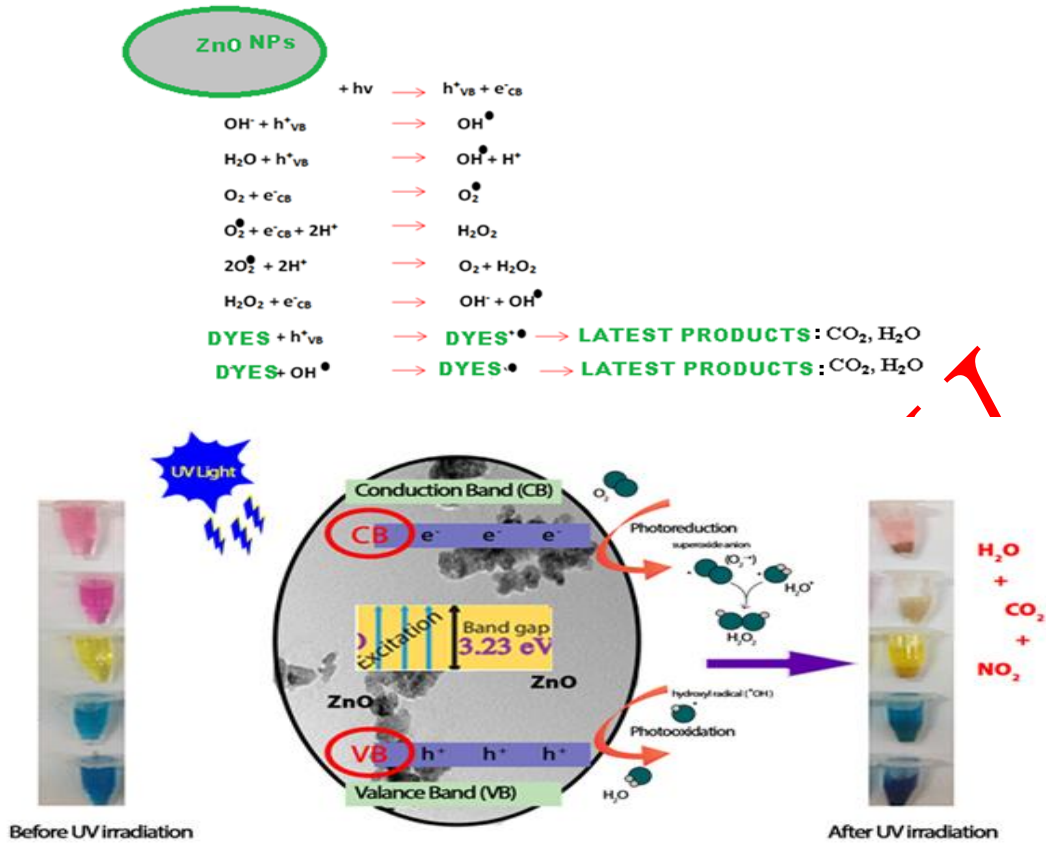


Figure 10. Illustration of the photocatalytic degradation process's mechanism

Turbidity caused higher values to be observed when the amount of dyestuff in the reaction mixture was measured using the UV-Vis spectrophotometric method. The first derivative method was employed to address the problem of being unable to precisely determine the dye concentration in the solution directly from absorbance measurements in turbid samples. This is why the derivative method is particularly useful for determining the dyestuff quantity in situations where turbidity is present or the background absorbance is either poorly defined or high. Especially in the spectra of BR46 (Figure 11), BV39 (Figure 12), and MB (Figure 13) dyes, these effects are seen quite a lot, but less in the spectra of BB3 (Figure 14) and BY28 (Figure 15) dyes, and this effect cannot be eliminated even if the samples are centrifuged. The reason for this may be the structure of the dyestuff and the amount of photocatalyst taken. As seen in Figures from 11 to 15, since decolorization is observed in the samples as a result of adsorption and photocatalytic degradation, while we should have read lower absorbance values, an increase in the absorption spectra was observed. When we take the derivative spectra, it is seen that this effect is eliminated and it is seen that correct results are obtained even though the samples are not centrifuged (Figures from 11 to 15).

Preparation of the calibration graphs and dyestuff solutions: The stock dyestuff aqueous solutions (100 mg/L) were diluted at the proper rates to produce standard dyestuff solutions. First derivative absorption spectra in the wavelength range of 300 nm -750 nm were used to measure first derivative absorbance values.

The photodecolorization efficiency, symbolized by the color removal, was calculated by detecting the peak amplitudes at 553 nm, 679 nm, and 667 nm wavelengths for BR46, MB, and BB3, respectively (Figures 11, 13, and 14). Peak amplitudes (1D values) in the recorded spectra for the BV39 dyestuff solutions (Figure 12) were measured at 572 nm for the purpose of determining the decolorization of BV39, whereas peak amplitudes (1D values) in the recorded spectra for the BY28 dyestuff solutions (Figure 15) were measured at 474 nm for the purpose of determining the decolorization of BY28. Plotting the first derivative absorbance data against concentration allowed the calibration graphs to be created. Equation (1) was used to calculate the decolorization efficiency (DE%), and the concentration values were taken from the

associated calibration graph. All measurements were carried out in duplicate, and the mean values have been used

$$\text{Decolorization efficiency: (DE \%)} = \frac{(C_0 - C_e)}{C_0} \times 100 \quad (1)$$

where C_0 and C_e represent, in mg/L, respectively, the adsorbate's initial and equilibrium (remaining non decolorized) liquid-phase concentrations.

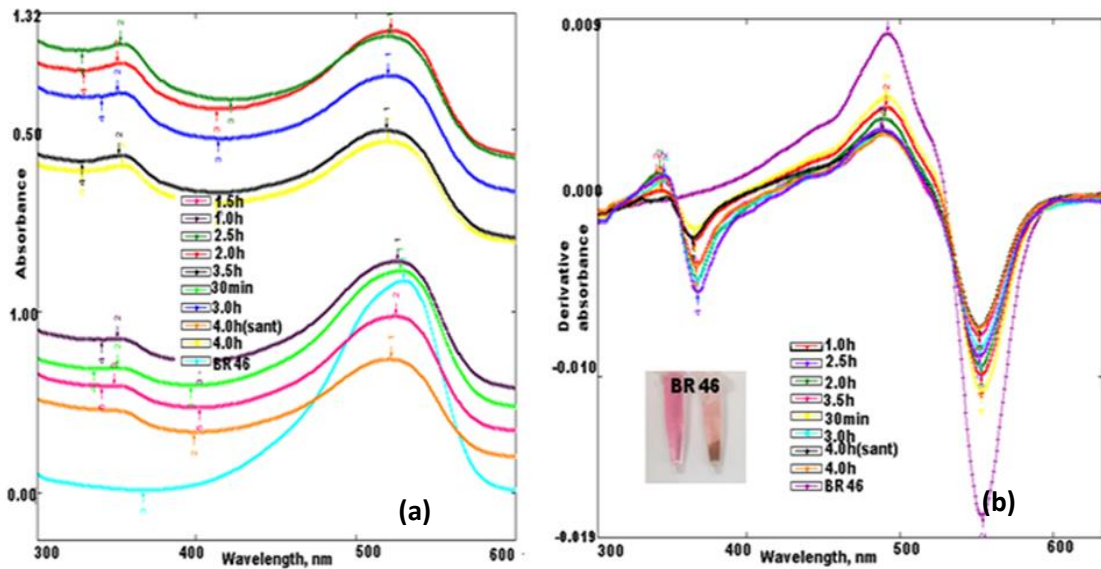


Figure 11 . (a) Absorption and (b) first derivative spectra of BR46 solution taken after stirred under UV-light for different time intervals (amount of CA-ZnO NPs: 0.05 g, dyestuff concentration: 10 $\mu\text{g/mL}$, inset; visual of observed color change)

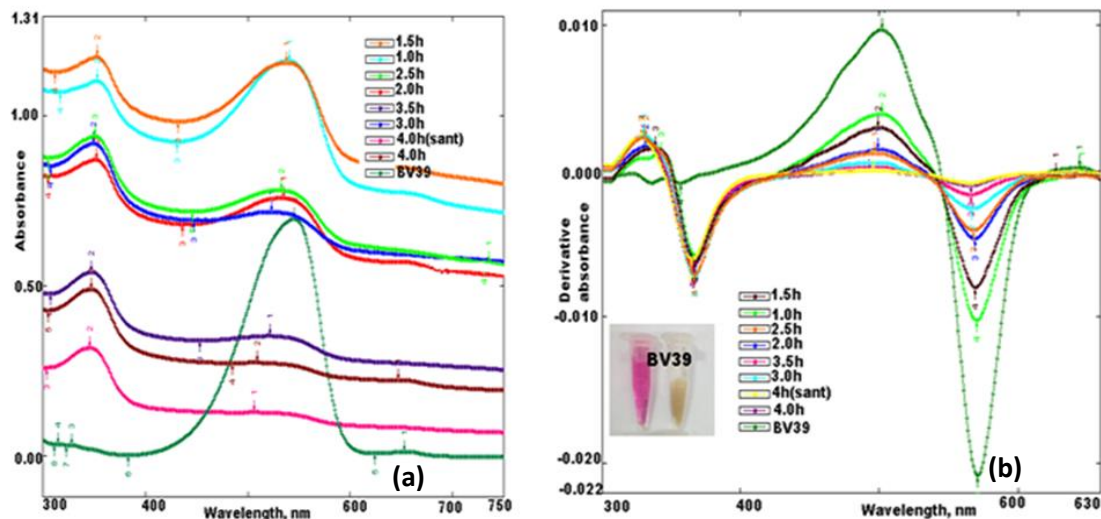


Figure 12 . (a) Absorption and (b) first derivative spectra of BV39 solution taken after stirred under UV-light for different time intervals (amount of CA-ZnO NPs: 0.05 g, dyestuff concentration: 10 $\mu\text{g/mL}$, inset; visual of observed color change)

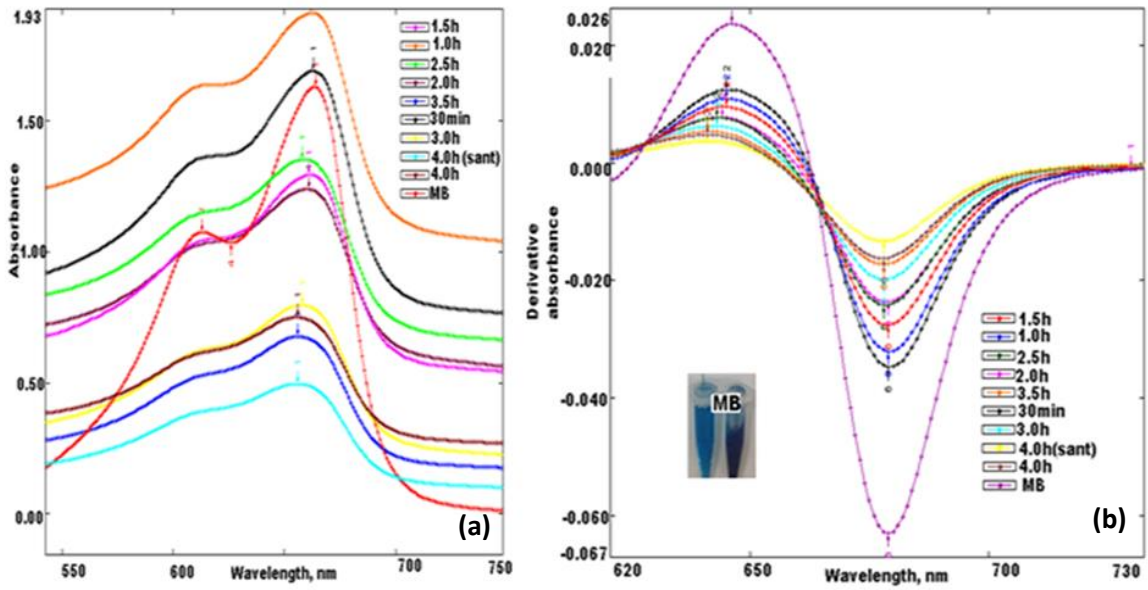


Figure 13 . The absorption and first derivative spectra of the MB solution after stirring under UV- light for various periods of time are shown in (a) and (b), respectively (amount of CA-ZnO NPs: 0.05 g, dyestuff concentration: 10 $\mu\text{g/mL}$, inset; visual of observed color change)

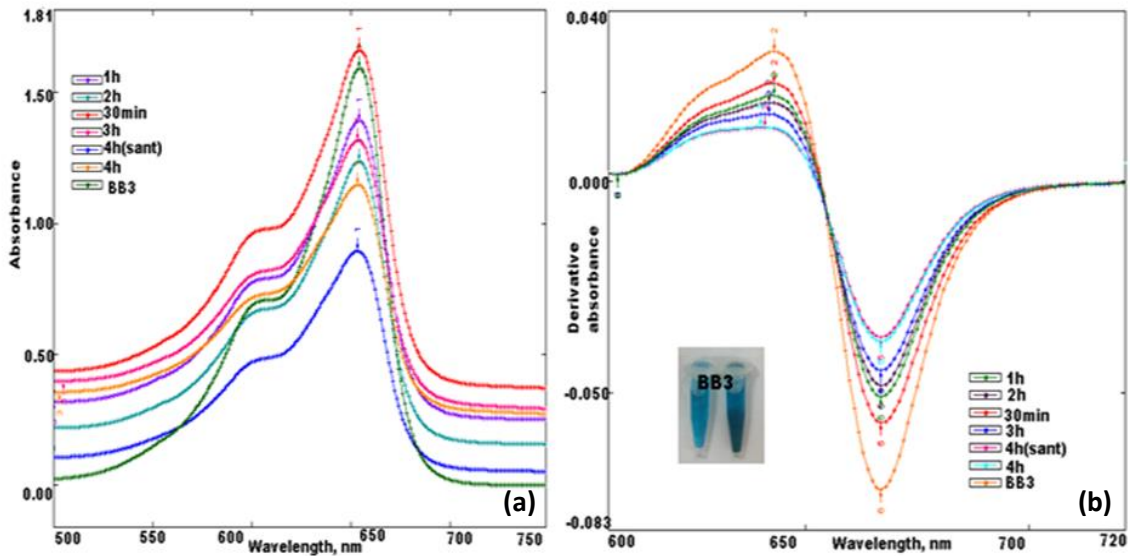


Figure 14 . (a) Absorption and (b) first derivative spectra of BB3 solution taken after stirred under UV- light for different time intervals (amount of CA-ZnO NPs: 0.05 g, dyestuff concentration : 10 $\mu\text{g/mL}$, inset; visual of observed color change)

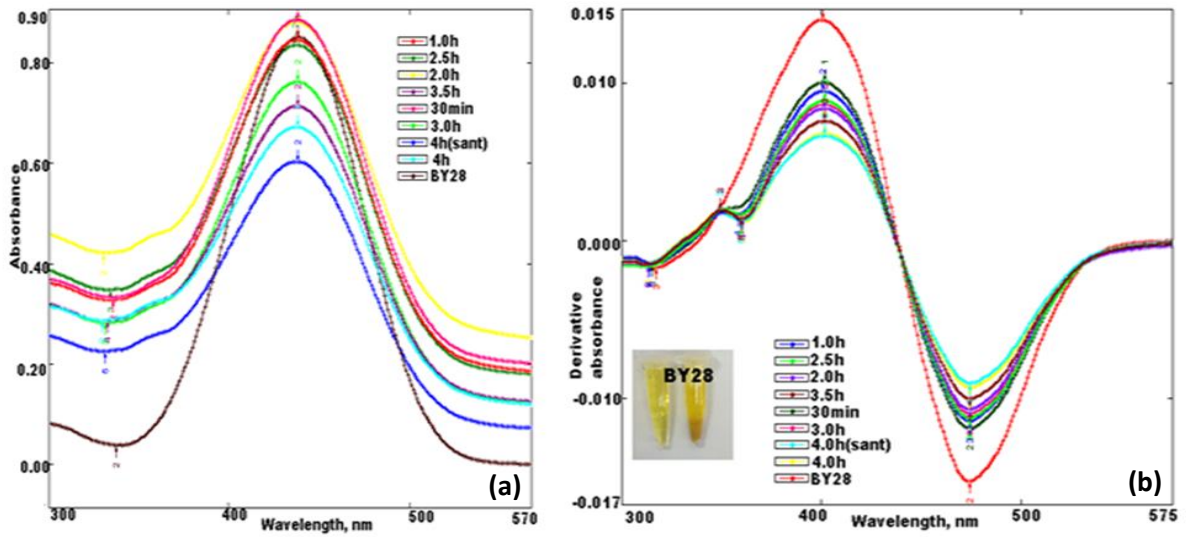


Figure 15. (a) Absorption and (b) first derivative spectra of BY28 solution taken after stirred under UV - light for different time intervals (amount of CA-ZnO NPs: 0.05 g, dyestuff concentration: 10 $\mu\text{g/mL}$, inset; visual of observed color change)

As observed in Figure 12 that the BV39 dyestuff did not adhere to CA-ZnO NPs due to adsorption, but the color was lightened as a result of photocatalytic degradation. When UV-Vis spectra of the other dyestuff solutions containing the same concentration of dye and photocatalyst (10 $\mu\text{g/mL}$ dyestuff + 0.05 g CA-ZnO NPs) were examined, it was determined that the color decreased less and the adsorption phenomenon was also observed (Figures 11, 13-15).

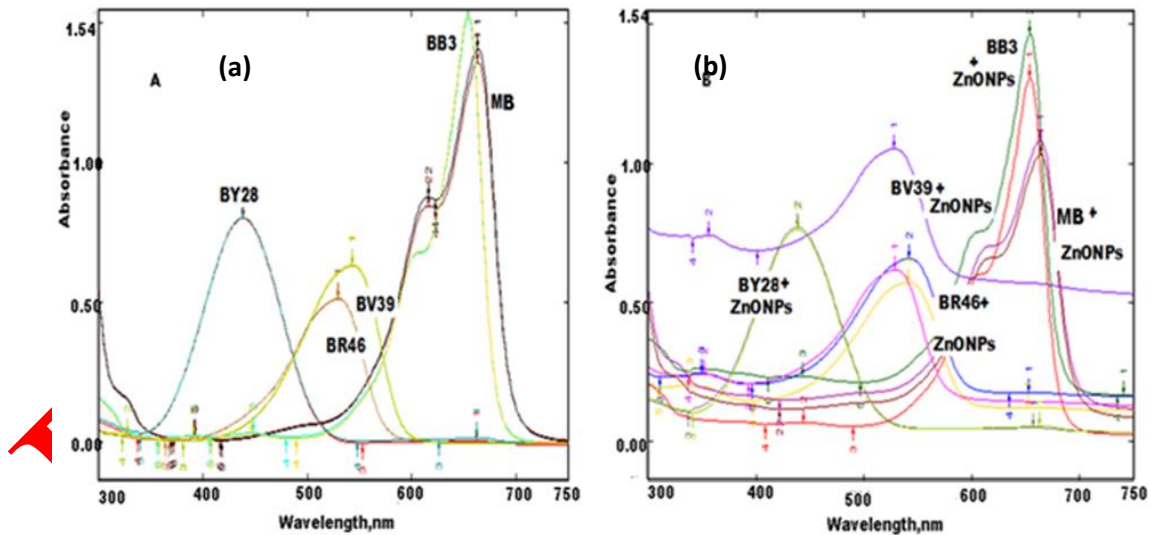


Figure 16. UV-Vis spectra of A) photocatalyst-free BY28, BV39, MB, BB3 and BR46 dyestuff solutions, B) BY 28, BV39, MB, BB3, and BR46 dyestuff solutions stirred for 1 h in dark and 7 h under daylight (amount of photocatalyst: 0.05 g, dyestuff concentration: 10 $\mu\text{g/mL}$)

Decolorization rates of dyestuff solutions for 10 $\mu\text{g/mL}$ concentration without adding nanophotocatalyst are the same values after 3 h and 7 h of stirred under daylight (Figure 16a). The decolorization rates found are; 4.0%, 6.8%, 5.2%, 4.8%, and 16.6% for BY28, BV39, MB, BB3, and BR46, respectively. After 7 h of stirred under UV- light found decolorization rates are 7.7%, 2.3%, 1.2% and 27.7% for BY28, MB, BB3 and BR46, respectively. For BV39, it was 7.9% after 3 h and 22% after 7 h (Data not shown). When we look at the photocatalytic degradation rates of dyestuff solutions with CA-ZnO NPs stirred under daylight, obtained values for BY28, MB, and BR46 dyestuff are the same for 3 h and 7 h. Values for decolorization

percentages are 13%, 36%, and 21.74%, respectively. For BB3, it was 12.0% after stirred 3 h and 22.0% after 7 h. For BV39, it was found 42.0% and 49.0% after stirred 3 h and 7 h, respectively (Figure 16b). Photocatalytic degradation percentages of 10 µg/mL dyestuff solutions with CA-ZnO NP after stirred for 1 h in darkness and 3 h under UV- light were 24.0%, 76.0%, 56.0%, 31.0%, and 26% for BY28, BV39, MB, BB3, and BR46, respectively and after 7h it was found as 53.0%, 100.0%, 77.0%, 74.0%, and 63% (Figure 17a). Dyestuff solutions with CA-ZnO NP after stirred for 1 h in darkness and 3 h under UV- light for dyes that were worked under UV- light, decolorization rates ranged from 24% to 77%, while color removal of up to 53% -100% was observed within 8 h (mixing for 1 h in darkness and 7 h under UV- light). Photodegradation completed in 7 h in aqueous solutions of dyestuffs revealed that nano ZnO particles have significant photocatalytic activity.

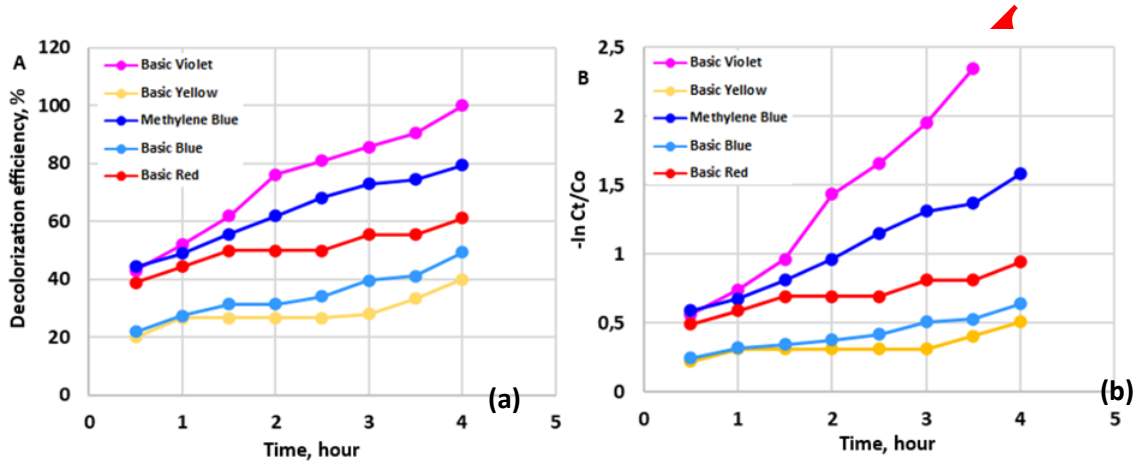


Figure 17. Diagram showing (a) the percentage of dyestuff decolorization and (b) the relationship between $-\ln C_t/C_0$ and the time needed to degrade dyestuff exposed to UV- light

A high decolorization rate has been observed in the dark within one hour, as shown in Figure 17a. For the decolorization of dyestuff by CA-ZnO NPs, the spectra displayed a direct relationship against time, and Figure 17b depicts a plot of $-\ln (C_t/C_0)$ as a function of response time. The values of the correlation coefficient (R^2) in the graphs were computed and are provided below. This demonstrated the photodegradation of dyes by CA-ZnO NPs under UV- light, with pseudo first-order kinetics. The high rate of adsorption is supported by correlation coefficient values higher than 0.9000. The optimal adsorption rate is indicated by correlation coefficients that are closer to 1.0000 in both situations. The results are consistent with the adsorption phenomenon observed for the dye BY28. It was revealed that the CA-ZnO NPs decolorize the dyestuff molecules in accordance with pseudo first-order kinetics. This result aligns with the findings of Neppolian et al. [38], who noted that most organic molecules are defined by the first-order kinetics of pseudo. As result, the dyestuffs' kinetics of degradation is as follows.

$y = 0.6058x + 0.1687$	$(R^2 = 0.9884)$	(For Basic Violet, from 0.5 to 4 h)
$y = 0.6058x + 0.1687$	$(R^2 = 0.9884)$	(For Basic Violet, from 0.5 to 8 h)
$y = 0.1031x + 0.1907$	$(R^2 = 0.9666)$	(For Basic Blue, from 0.5 to 4 h)
$y = 0.1793x + 0.0367$	$(R^2 = 0.9367)$	(For Basic Blue, from 0.5 to 8 h)
$y = 0.0591x + 0.2029$	$(R^2 = 0.7175)$	(For Basic Yellow, from 0.5 to 4 h)
$y = 0.1135x + 0.0931$	$(R^2 = 0.9009)$	(For Basic Yellow, from 0.5 to 8 h)
$y = 0.1100x + 0.4681$	$(R^2 = 0.9255)$	(For Basic Red, from 0.5 to 4 h)
$y = 0.1307x + 0.4263$	$(R^2 = 0.9766)$	(For Basic Red, from 0.5 to 8 h)
$y = 0.2876x + 0.4094$	$(R^2 = 0.9917)$	(For Methylene Blue, from 0.5 to 4 h)
$y = 0.1646x + 0.6583$	$(R^2 = 0.8288)$	(For Methylene Blue, from 0.5 to 8 h)

A comparison of the results with those reported was conducted in Table 2 by taking into account time and yield %. The results are consistent with the earlier research, as can be seen.

Table 2. Studies on the photocatalytic activities of green synthesized zinc oxide nanoparticles

Reducing and capping agent	Dyestuff	Light type	Time (min)	Yield %	Reference
<i>Scutellaria baicalensis</i> root	Methylene blue and Methyl orange	UV- light	21	96.6–98.2	[39]
<i>Thymus vulgaris</i>	Methylene blue	UV- light	30	96	[40]
<i>Hydnocarpus alpina</i>	Indigo carmine	Sunlight	-----	83	[41]
<i>Peltophorum pterocarpum</i>	Methylene blue	Sunlight	120	95	[37]
<i>Cynara scolymus</i>	Methylene blue	UV- light	240	80	[42]
<i>Lagerstroemia speciosa</i>	Methyl orange	Sunlight	100	93.5	[43]
¹ <i>Citrus sinensis</i> ² <i>Citrus aurantifolia</i> ³ <i>Citrus paradisi</i> ⁴ <i>Lycopersicon esculentum</i>	Methylene blue	UV- light	180	¹ 95 ² 97 ³ 77 ⁴ 97	[44]
<i>Pithecellobium dulce</i>	Methylene blue	UV- light	120	63	[45]
<i>Trianthema portulacastrum</i>	Synzol ultramarine -KBF	Sunlight	159	91	[46]
<i>Boswellia</i> gum	Methylene blue	UV- light	180	70	[47]
<i>Calliandra haematocephala</i>	Methylene blue	Sunlight	270	88	[10]
<i>Cupressus arizonica</i>	BY28 ^a MB ^b BR46 ^c BV39 ^d BB3 ^e	UV- light	420	53.0 % ^a 77.0 % ^b 63 % ^c 100.0 % ^d 74.0 % ^e	This study

Footnotes: 1, 2 and 3 refer to the different plants and a, b, c, d, and e refer to the different dyestuff were studied

3.4. Antibacterial Efficiency of CA-ZnO NPs

Using the disc diffusion method, the antibacterial effectiveness (AE) of CA-ZnO NPs against *E. coli* and *S. aureus* has been demonstrated in Figure 18 and antibacterial effectiveness results are given in Table 3. It was determined that ZnO nanoparticles were effective against both bacteria and formed an inhibition zone varying between 10.0 - 1.0 mm against *S. aureus* and *E. coli*. The results of AE showed that *E. coli* is more susceptible to CA-ZnO nanoparticles toxicity compare to *S. aureus*. The aqueous extract of the leaves (sample 3) did not show AE against both bacteria, while the ethanolic extract of the leaves (sample 2) showed AE against both bacteria. Ethyl alcohol extract of the cones (example 1) showed AE only against *E. coli*. ZnO NPs (sample 4, 5, 10, 12) produced from the aqueous extract of leaves showed AE only against *E. coli*. ZnO NPs produced from the ethanolic extract of leaves and calcined at low temperature did not show AE (sample 9), while those calcined at high temperature (sample 14) showed AE against both bacterial strains. ZnO NPs produced from the aqueous extract of the cones also did not show AE against both bacterial strains (except for sample 6). ZnO NPs produced from the ethyl alcohol extract of cones and calcined at different temperatures showed AE against *E. coli* (sample 13), *S. aureus* (sample 8) and two bacterial species (sample 7). Photocatalytic studies were continued with the aqueous ethanolic extract of the leaf+cone mixture.

Yusof et al. stated that the ZnO nanoparticles they obtained exhibited 16 and 13 mm inhibition zones against *S. aureus* and *E. coli* respectively [18]. ZnO NPs show antibacterial effect both gram+ and gram- bacteria strains. In the literature, it has been mentioned that while the surface area and nanoparticle concentration are first-order effective on antibacterial activity, the effect of crystal structure and particle shape is low [48]. Singh and his work group reported that particle size is an important parameter because the extraordinary physicochemical properties are more pronounced at smaller sizes, and the ability of ZnO nanoparticles, which are smaller in size compared to the pore size in bacteria, to pass through the cell membrane depends on the size of the nanoparticles [49]. On the other hand, it was observed that the antibacterial activity of ZnO NPs increased against various gram+ and gram-bacterial strains with decreasing particle size and increasing concentration [7, 50].

Ramesh et al., in their study, executed the green production of ZnO nanoparticles by bioreducing leaves extract of *Solanum nigrum*. They obtained nanoparticles of 20-30 nm in dimensions and wurtzite hexagonal structure. The antibacterial efficiency of these particles were tested against human pathogen gram+ (*S. aureus*, 18 mm) and gram- (*Salmonella paratyphi*, 17 mm), *Vibrio cholerae* (11 mm), *E. coli* (7 mm) bacteria and it was determined that they have high antimicrobial effect. But it has been demonstrated that the size of ZnO nanoparticles affects their antibacterial effectiveness; it was found that the smaller the dimensions, the greater the antibacterial effectiveness [51]. Madan et al. showed that at a certain concentration, ZnO NPs produced by using neem plant concentrated (*Azadirachta indica*) were specific against *Klebsiella aerogenes* (NCIM-2098) and *S. aureus* (NCIM-5022) but not effective against *E. coli* (NCIM-5051) and *Pseudomonas aeruginosa* (NCIM-2242). The differences in the structural and compositional content of the bacterial cell membrane of these four bacterial species, as well as the surface morphology of the metal oxide NPs, have been attributed to this selective efficiency on particular bacteria [31]. According to Nilavukkarasi et al., gram- bacteria have a more complex chemical makeup in terms of both structure and function than gram+ types [52]. Kumar et al. stated that Zn^{2+} delay cell growth in gram+ bacterial cells, interfere with biochemical processes and perform cell death in a simpler way [53]. In our study, differences were observed in the antibacterial sensitivity of *E. coli* and *S. aureus*.

The antibacterial properties of ZnO NPs derived from *Camellia sinensis* (green tea) have been assessed in a further study carried out with extracts extracted from these plants. The study showed that the plant extract had sensitivity to bacteria, with an inhibition zone of 32 ± 0.050 mm for *P. aeruginosa* and 25 ± 0.100 mm for *S. aureus*. The highest activity against the tested bacteria was observed in the extract prepared with methanol. While the ethanolic and aqueous extract showed almost similar activity after the methanolic

extract, but no activity was recorded in the chloroform extract [8]. As seen in Table 3, nanoparticles obtained by using ethyl alcohol extracts are more effective against bacteria.

The high temperature treatment has a significant impact on the antibacterial activity of ZnO particles. Processing at higher calcination temperatures provides higher activation energy for diffusion and this effect causes crystalline ZnO NPs to grow and gain a lower property [48, 54]. As seen in Table 3, ZnO nanoparticles dried or ashed at different temperatures show different antibacterial activity against both types of bacteria.

Table 3. Inhibition zone diameters (mm) of biosynthesized CA-ZnO NPs

Sample code number	Samples (100 μ L)	<i>S.aureus</i>	<i>E.coli</i>
1	Cone ethanol extract (CEE)	0	11
2	Leaves ethanol extract (LEE)	11	11
3	Leaves water extract (LWE)	0	0
4	ZnO NP produced with LWE Dried vacuum at 60°C, 4 h	0	11
5	ZnO NP produced with LWE Dried vacuum at 60°C, 2 h	0	11
6	ZnO NP produced with CWE Dried vacuum at 60°C, 4 h	0	11
7	ZnO NP produced with CEE+LEE(1:1,v:v) Dried vacuum at 60°C, 4 h	10	10
8	ZnO NP produced with CEE Dried oven at 150°C, 6 h	11	0
9	ZnO NP produced with LEE Dried oven at 150°C, 6 h	0	0
10	ZnO NP produced with LWE Dried oven at 150°C, 6 h	0	10
11	ZnO NP produced with CWE Dried oven at 150°C, 6 h	0	0
12	ZnO NP produced with LWE Dried oven at 400°C, 2 h	0	11
13	ZnO NP produced with CEE Dried oven at 400°C, 2 h	0	11
14	ZnO NP produced with LEE Dried oven at 400°C, 2 h	11	10
15	ZnO NP produced with CWE Dried oven at 400°C, 2 h	0	0

Footnotes: CEE: Cone ethyl alcohol extract, LEE: Leaves ethyl alcohol extract, CWE: Cone water extract, LWE: Leaves water extract

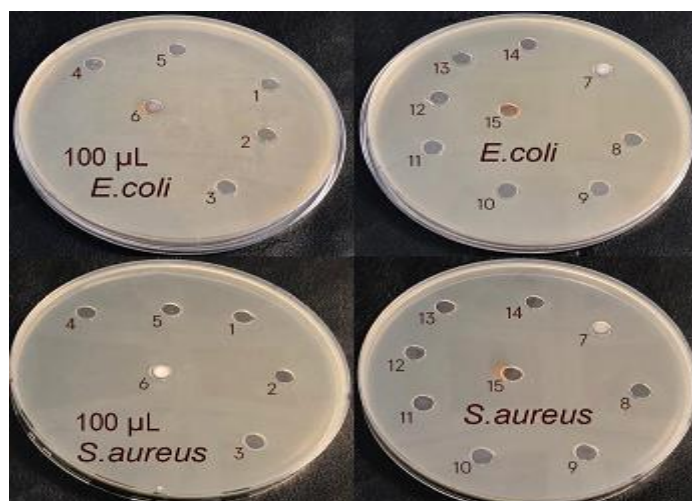


Figure 18. Images of the antibacterial activity studies of biosynthesized CA-ZnO NPs

4. RESULTS

Metal oxide nanoparticles are materials that have attracted great interest in the scientific world in recent years and have been studied extensively. Classical synthesis methods of metal oxide nanoparticles include many disadvantages such as being complex and very expensive, requiring the use of toxic substances, and not being suitable for pharmacological and biomedical applications. In this work, ZnO NPs were produced and the applicability of these green synthesized nanoparticles as a suitable photocatalyst in the treatment of water and also as a safe antibacterial agent was investigated. For the first time, economical, quick and eco-friendly method was used for producing ZnO NPs in this study using ethanol and water extracts of *Cupressus arizonica* leaves and cones. The new eco-friendly synthesis method is a practical method for industrial-scale production. The developed method does not require the use of harmful and toxic solvents. This environmentally friendly synthesis technique could be a competitive alternative to traditional chemical and physical techniques.

In this study, zinc acetate dihydrate (Zn-Ac) and *Cupressus arizonica* leaves, cones and leaves + cones mixture were used for the synthesis. Zn-Ac/CA ratio of 1:1 (v/v), reaction temperature of 60°C, reaction time of 180 min, pH of 12, calcined temperature of 400°C, calcined time of 120 min are the operating conditions for bioproduction. SEM, TEM, and HR-TEM have been used to characterise the particle size and surface morphology of green synthesized CA-ZnO NPs. Using FT-IR, functional groups have been identified in biosynthesized CA-ZnO NPs. CA-ZnO NPs produced by using aqueous ethanolic extract of leaves + cones mixture were used in the photocatalytic studies. In determining the photocatalytic activity of the produced CA-ZnO NPs, BY28, BV39, MB, BB and BR46 dyestuff, which are used in dyeing processes in the textile industry and are ecologically harmful, were used as model pollutants. The investigation results showed that produced CA-ZnO NPs were able to effectively decolorize the dye solutions and the efficiency was found to be 53.0% for BY28, 100.0 % for BV 39, 77.0% for MB, 74.0% for BB and 63% for BR46. Photodegradation completed in 7 h in aqueous solutions of dyestuffs revealed that CA-ZnO NPs have significant photocatalytic activity. Decolorization of the dyestuff molecules followed the pseudo first-order kinetics. The high adsorption rate was supported by a correlation coefficient of more than 0.9000. Nanoparticles may have a vital role of wastewater treatment at the present time, when there are inadequate water supplies worldwide. This article describes the green photocatalytic pathway for removal of BY28, BV39, MB, BB and BR46 dyestuffs from aqueous solutions using CA-ZnO NPs with excellent photocatalytic abilities while highlighting its potential application in water treatment. In the forthcoming years, water shortages can be avoided with the help of this research. In photocatalytic studies, when absorption spectra used to calculate the dye concentration in the reaction mixture, higher values obtained due to turbidity. In this study, it was found that taking derivative spectra gave more accurate results in spectrophotometric monitoring of photocatalysis reactions. The CA-ZnO NPs hold great promise for removing BY28, BV39, MB, BB, and BR46 dyestuffs from aqueous solutions due to their advantages of

being produced from a low-cost source, high adsorption capacity, and high photocatalytic efficiency. CA-ZnO NPs formed an inhibition zone varying between 10.0 - 11.0 mm against *S. aureus* and *E. Coli*. CA-ZnO NPs obtained by using ethanolic extract are more effective against bacteria and ZnO nanoparticles dried or ashed at different temperatures showed different antibacterial activity against both types of bacteria.

CONFLICTS OF INTEREST

No conflict of interest was declared by the authors.

REFERENCES

- [1] Narayanan, K. B., Sakthivel, N., "Biological synthesis of metal nanoparticles by microbes", *Advances in Colloid and Interface Science*, 156:1-13, (2010).
- [2] Bar, H., Bhui, D. K., Sahoo, G. P., Sarkar, P., De, S. P., Misra, A., "Green synthesis of silver nanoparticles using latex of *Jatropha curcas*", *Colloids and Surfaces A: Physicochemical and Engineering Aspects*, 339: 134-139, (2009).
- [3] Thombre, R., Chitnis A., Kadam V., Bogawat Y., Colaco R., Kale A., "A facile method for synthesis of biostabilized silver nanoparticles using *Eicchornia crassipes* water hyacinth (Mart.) Solms (water hyacinth)", *Indian Journal of Biotechnology*, 13: 337-341, (2014).
- [4] Abbasi, B. A., Iqbal, J., Ahmad, R., Zia, L., Kanwal, S., Mahmood, T., Chen, J. T. "Bioactivities of *Geranium wallichianum* Leaf Extracts Conjugated with Zinc Oxide Nanoparticles", *Biomolecules*, 10, 38: 1-19, (2020).
- [5] Nava, O. J., Luque, P. A., Gómez-Gutiérrez, C. M., Vilchis-Nestor, A. R., Castro-Beltrán, A., Mota-González, M. L., Olivás, A., "Influence of *Camellia sinensis* extract on Zinc Oxide nanoparticle green synthesis", *Journal of Molecular Structure*, 1134: 121-125, (2017).
- [6] Kumar, A. K., Saila, E. S., Narang, P., Aishwarya, M., Raina, R., Gautam, M., Shankar, E. G., "Biofunctionalization and biological synthesis of the ZnO nanoparticles: the effect of *Raphanus sativus* (white radish) root extract on antimicrobial activity against MDR strain for wound healing applications", *Inorganic Chemistry Communications*, 100: 101-106, (2019).
- [7] Ogunyemi, S. O., Abdallah, Y., Zhang, M., Fouad, H., Hong, X., Ibrahim, E., Li, B., "Green synthesis of zinc oxide nanoparticles using different plant extracts and their antibacterial activity against *Xanthomonas oryzae* pv. *Oryzae*", *Artificial Cells, Nanomedicine and Biotechnology*, 47(1): 341-352, (2019).
- [8] Shah, R. K., Boruah, F., Parween, N., "Synthesis and characterization of ZnO nanoparticles using leaf extract of *Camellia sinensis* and evaluation of their antimicrobial efficacy", *International Journal of Current Microbiology and Applied Sciences*, 4(8): 444-450, (2015).
- [9] Ahmad, W., Kalra, D., "Green Synthesis, Characterization and Anti microbial Activities of ZnO Nanoparticles Using *Euphorbia hirta* leaf extract", *Journal of King Saud University-Science*, 32(4): 2358-2364, (2020).
- [10] Vinayagam, R., Selvaraj, R., Arivalagan, P., Varadavenkatesan, T., "Synthesis, characterization and photocatalytic dye degradation capability of *Calliandra haematocephala*-mediated zinc oxide nanoflowers", *Journal of Photochemistry and Photobiology B: Biology*, 203: 111760, (2020).
- [11] Yuvakkumar, R., Suresh, J., Nathanael, A. J., Sundrarajan, M., Hong, S. I., "Novel green synthetic strategy to prepare ZnO nanocrystals using rambutan (*Nephelium lappaceum* L.) peel extract and its antibacterial applications", *Materials Science and Engineering:C*, 41: 17-27, (2014).

- [12] Thema, F. T., Manikandan, E., Dhlamini, M. S., Maaza, M., “Green synthesis of ZnO nanoparticles via *Agathosma betulina* natural extract”, *Materials Letters*, 161: 124-127, (2015).
- [13] Ustun Ozgur, M., Duygulu, O., Altikatoglu Yapaoz, M., “Investigation of antibacterial and photocatalytic efficiency of green ZnO nanoparticles that synthesized with *Celosia Cristata* flower extract”, *Turkish Journal of Chemistry*, 46(1): 59-85, (2022).
- [14] Akbar, A., Sadiq, M. B., Ali, I., Muhammad, N., Rehman, Z., Khan, M. N., Anal, A. K., “Synthesis and antimicrobial activity of zinc oxide nanoparticles against foodborne pathogens *Salmonella typhimurium* and *Staphylococcus aureus*”, *Biocatalysis and Agricultural Biotechnology*, 17: 36-42, (2019).
- [15] Agarwal, H., Kumar, S. V., Rajeshkumar, S., “A review on green synthesis of zinc oxide nanoparticles—An eco-friendly approach”, *Resource-Efficient Technologies*, 3(4): 406-413, (2017).
- [16] Król, A., Pomastowski, P., Rafińska, K., Railean-Plugaru, V., Buszewski, B., “Zinc oxide nanoparticles: Synthesis, antiseptic activity and toxicity mechanism”, *Advances in Colloid and Interface Science*, 249: 37-52, (2017).
- [17] Sasidharan, S., Raj, S., Sonawane, S., Pinjari, D., Pandit, A. B., Saudagar, P., “Nanomaterial synthesis: chemical and biological route and applications”, In *Nanomaterials Synthesis* (pp. 27-51). Elsevier. (2019).
- [18] Yusof, N. A. A., Zain, N. M., Pauzi, N., “Synthesis of ZnO nanoparticles with chitosan as stabilizing agent and their antibacterial properties against Gram-positive and Gram-negative bacteria”, *International Journal of Biological Macromolecules*, 124: 1132-1136, (2019).
- [19] Ahmadi Shadmehri, A., Namvar, F., “A Review on Green Synthesis, Cytotoxicity Mechanism and Antibacterial Activity of ZnO-NPs”, *International Journal of Research in Applied and Basic Medical Sciences*, 6(1): 23-31, (2020).
- [20] Sabir, S., Arshad, M., Chaudhari, S. K. “Zinc oxide nanoparticles for revolutionizing agriculture: synthesis and applications”, *The Scientific World Journal*, 2014: 1-8, (2014).
- [21] Mochane, M. J., Motloun, M. T., Mokhena, T.C., Mofokeng, T.G., “Morphology and Photocatalytic Activity of Zinc Oxide Reinforced Polymer Composites: A Mini Review”, *Catalysts*, 12(11): 1439, (2022).
- [22] Ramos, P.G., Sánchez, L.A., Rodriguez J.M., “Review paper: sol–gel and hybrid materials for optical, photonic and optoelectronic applications, A review on improving the efficiency of photocatalytic water decontamination using ZnO nanorods”, *Journal of Sol-Gel Science and Technology*, 102:105–124, (2022).
- [23] Servi Uçucu Yağı: Faydaları, Özellikleri ve Kullanımları. <https://aromaterapio.com>
- [24] Bauer A.W., Kirby W.M., Sherris J.C., Turck M., “Antibiotic Susceptibility Testing by a Standardized Single Disc Method”, *American Journal of Clinical Pathology*, 45(4): 493-6, (1966).
- [25] Ezealisiji, K.M., Siwe-Noundou, X., Maduelosi, B., Nwachukwu, N.W., Krause, R.W.M., “Green Synthesis of Zinc Oxide Nanoparticles Using *Solanum torvum* (L) Leaf Extract and Evaluation of the Toxicological Profile of the ZnO Nanoparticles-Hydrogel Composite in Wistar Albino Rats”, *International Nano Letters*, 9: 99–107, (2019).
- [26] Suresh, J., Pradheesh, G., Alexramani, V., Sundrarajan, M., Hong, S.I., “Green Synthesis and Characterization of Zinc Oxide Nanoparticle Using Insulin Plant (*Costus pictus* D. Don) and Investigation of its Antimicrobial as Well as Anticancer Activities”, *Advances in Natural Sciences:*

- Nanoscience and Nanotechnology, 9(1): 015008–015016, (2018).
- [27] Safawo T., Sandeep B.V., Pola, S., Tadesse, A., “Synthesis and characterization of zinc oxide nanoparticles using tuber extract of anchote (*Coccinia abyssinica* (Lam.) Cong.) for antimicrobial and antioxidant activity assessment”, *OpenNano*, 3: 56-63, (2018).
- [28] Donmez S., “Green Synthesis of Zinc Oxide Nanoparticles Using Zingiber Officinale Root Extract and Their Applications in Glucose Biosensor”, *El-Cezeri Journal of Science and Engineering*, 7 (3): 1191-1200, (2020).
- [29] Oman, Z., Harry, B., Nuryatini, H., (2013). “ Synthesis of ZnO nanoparticles for microwave-induced rapid catalytic decolorization of congo red dye ”, *Advanced Materials Letters*, 4: 662-667, (2013).
- [30] Nagarajan, S., Kuppusamy, K. A., “Extracellular synthesis of zinc oxide nanoparticle using seaweeds of gulf of Mannar India”, *Journal of Nanobiotechnology*, 11(1): 1-11, (2013).
- [31] Madan, H.R., Sharma, S.C., Udayabhanu., Suresh, D., Vidya, Y.S., Nagabhusana, H., Rajanaik, H., Anantharaju, K.S., Prashantha, S.C., Sadananda Maiya, P., “Facile Green Fabrication of Nanostructure ZnO Plates, Bullets, Flower, Prismatic Tip, Closed Pine cone: Their Antibacterial, Antioxidant, Photoluminescent and Photocatalytic Properties”, *Spectrochimica Acta Part A: Molecular and Biomolecular Spectroscopy*, 152: 404-416, (2016).
- [32] Elumalai, K., Velmurugan, S., Ravi, S., Kathiravan, V., Adaikala Raj, G., “Bio-Approach: Plant Mediated Synthesis of ZnO Nanoparticles and Their Catalytic Reduction of Methylene Blue and Antimicrobial Activity”, *Advanced Powder Technology*, 26(6): 1639-1651, (2015).
- [33] Srinivasa Rao, N., Basaveswara Rao, M.V., “Structural and Optical Investigation of ZnO Nanopowders Synthesized from Zinc Chloride and Zinc Nitrate”, *American Journal of Materials Science*, 5: 66-68, (2015).
- [34] Zhang, J., Tian, B., Wang, L., Xing, M., Lei, J., “Mechanism of Photocatalysis. In: Photocatalysis”, *Lecture Notes in Chemistry*, vol 100. Springer, Singapore, (2018).
- [35] Saravanan, R., Gracia, F., Stephen, A., “Basic Principles, Mechanism, and Challenges of Photocatalysis. In: Khan, M., Pradhan, D., Sohn, Y. (eds) *Nanocomposites for Visible Light-induced Photocatalysis*”, *Springer Series on Polymer and Composite Materials*. Springer, Cham. (2017).
- [36] Ong, C.B., Ng, L.Y., Mohammad, A. W., “A review of ZnO nanoparticles as solar photocatalysts: synthesis, mechanisms and applications”, *Renewable and Sustainable Energy Reviews*, 81: 536-551, (2018).
- [37] Pal, S., Sridevi, H., Varadavenkatesan, T., Vinayagam, R., Selvaraj, R., “Photocatalytic zinc oxide nanoparticles synthesis using *Peltophorum pterocarpum* leaf extract and their characterization”, *Optik*, 185: 248-255, (2019).
- [38] Neppolian, B., Sakthivel, S., Arabindoo, B., Palanichamy, M., Murugesan, V., “Degradation of textile dye by solar light using TiO₂ and ZnO photocatalysts *Journal of Environmental Science and Health Part A Toxic/ Hazardous Substances & Environmental Engineering*”, 34(9):1829-1838, (2008).
- [39] Chen, L., Batjikh, I., Hurh, J., Han, Y., Huo, Y., Ali, H., Li, J.F., Rupa, E.J. Ahn, J.C. Mathiyalagan, R., “Green synthesis of zinc oxide nanoparticles from root extract of *Scutellaria baicalensis* and its photocatalytic degradation activity using methylene blue”, *Optik*, 184: 324–329, (2019).

- [40] Zare, M., Namratha, K., Thakur, M. S., Byrappa, K., “Biocompatibility assessment and photocatalytic activity of bio-hydrothermal synthesis of ZnO nanoparticles by *Thymus vulgaris* leaf extract”, *Materials Research Bulletin*, 109: 49-59, (2019).
- [41] Ganesh, M., Gil Lee, S., Jayaprakash, J., Mohankumar, M., Jang, H.T., “Hydnocarpus alpina Wt extract mediated green synthesis of ZnO nanoparticle and screening of its anti-microbial, free radical scavenging, and photocatalytic activity”, *Biocatalysis and Agricultural Biotechnology*, 19: 101129, (2019).
- [42] Şendal, K., Özgür, M., Gülen, F. J., “Biosynthesis of ZnO photocatalyst and its application in photocatalytic degradation of methylene blue dyestuff”, *Journal of Dispersion Science and Technology*, 1-14, (2022).
- [43] Saraswathi, V.S., Tatsugi, J., Shin, P.K., Santhakumar, K., “Facile biosynthesis, characterization, and solar assisted photocatalytic effect of ZnO nanoparticles mediated by leaves of *L. Speciosa*”, *Journal of Photochemistry and Photobiology B: Biology*, 167: 89-98, (2017).
- [44] Nava, O. J., Soto-Robles, C. A., Gómez-Gutiérrez, C. M., Vilchis-Nestor, A. R., Castro-Beltrán, A., Olivas, A., Luque, P. A., “Fruit peel extract mediated green synthesis of zinc oxide nanoparticles”, *Journal of Molecular Structure*, 1147: 1-6, (2017).
- [45] Madh Madhumitha, G., Fowsiya, J., Gupta, N., Kumar, A., Singh, M., “Green synthesis, characterization and antifungal and photocatalytic activity of *Pithecellobium dulce* peel-mediated ZnO nanoparticles”, *Journal of Physics and Chemistry of Solids*, 127: 43-51, (2019).
- [46] Khan, Z. U. H., Sadiq, H. M., Shah, N. S., Khan, A. U., Muhammad, N., Hassan, S. U., Ullah, F., “Greener synthesis of zinc oxide nanoparticles using *Trianthema portulacastrum* extract and evaluation of its photocatalytic and biological applications”, *Journal of Photochemistry and Photobiology B: Biology*, 192: 147-157, (2019).
- [47] Nourbakhsh, M., Darroudi, M., Gholizadeh, M., “Role of bio-derived zinc oxide nanoparticles in antifungal and photocatalytic activities”, *Research on Chemical Intermediates*, 46(1): 243-252, (2020).
- [48] Zhang, L., Jiang, Y., Ding, Y., Povey, M., York, D., “Investigation into the antibacterial behaviour of suspensions of ZnO nanoparticles (ZnO nanofluids)”, *Journal of Nanoparticle Research*, 9(3): 479-489, (2007).
- [49] Singh, A. K., Pal, P., Yadav, T. P., Gupta, V., Singh, S. P., “Green synthesis, characterization and antimicrobial activity of zinc oxide quantum dots using *Eclipta alba*”, *Materials Chemistry and Physics*, 203: 40-48, (2018).
- [50] Awwad, A. M., Amer, M. W., Salem, N. M., Abdeen, A. O., “Green synthesis of zinc oxide nanoparticles (ZnO-NPs) using *Ailanthus altissima* fruit extracts and antibacterial activity”, *Chemistry International*, 6(3): 151-159, (2020).
- [51] Ramesh, M., Anbuvaran, M., Viruthagiri, G., “Green synthesis of ZnO nanoparticles using *Solanum nigrum* leaf extract and their antibacterial activity”, *Spectrochimica Acta Part A: Molecular and Biomolecular Spectroscopy*, 136: 864-870, (2015).
- [52] Nilavukkarasi, M., Vijayakumar, S., Prathipkumar, S., “*Capparis zeylanica* mediated bio-synthesized ZnO nanoparticles as antimicrobial, photocatalytic and anti-cancer applications”, *Materials Science for Energy Technologies*, 3: 335-343, (2020).
- [53] Kumar, R., Umar, A., Kumar, G., Nalwa, H. S., “Antimicrobial properties of ZnO nanomaterials: A review”, *Ceramics International*, 43(5): 3940-3961, (2017).

- [54] Azizi, S., Mohamad, R., Bahadoran, A., Bayat, S., Rahim, R. A., Ariff, A., Saad, W. Z., “Effect of annealing temperature on antimicrobial and structural properties of bio-synthesized zinc oxide nanoparticles using flower extract of *Anchusa italica*”, *Journal of Photochemistry and Photobiology B: Biology*, 161:441-449, (2016).

EARLY VIEW